Optimization of Piezo-Driven Jet Valve Dispensing Process for the Geometrical Control of Printed Sensors Based on Silver and MXene Inks

Michela Borghetti, *Member, IEEE*, Valeria Nicolosi, Emilio Sardini, *Member, IEEE*, Mauro Serpelloni, *Member, IEEE*, and Dahnan Spurling

***Abstract*— Printed sensors offer unique benefits—highly customizable designs, low-cost prototyping, and a wide range of materials and properties—which can be exploited. Piezo-driven jet valve dispensing is a printing technique suitable for the fabrication of sensors and electronics directly on the surfaces (both 2-D and 3-D) of smart objects and devices but needs additional analysis and study. In this work, we studied the influence of printing parameters on the performance of the Nordson PICO Jetting system mounted on the Neotech PJ15X machine by depositing a silver ink, typically used for the fabrication of sensors and interconnections, and a $Ti_3C_2T_X$ ink, a very promising 2-D material in the sensing and electronics fields for its extraordinary physical, electrical, chemical, and mechanical properties. A tuning approach was proposed to tune the printing parameters correctly. The profiles of the cross sections of printed lines were evaluated, including the process variability, when the values of the printing parameters were changed. In the case of $Ti_3C_2T_X$, the improper setting of the printing setup caused undesired spots and irregular lines. The optimal settings for the printing setup were found for each ink, reaching a variability in the profile of 1.5%.**

***Index Terms*— Flexible electronics, piezoelectric jetting, printed electronics (PE), printing, resistive sensors, sensors.**

I. Introduction

PRINTED electronics (PE) has recently attracted the attention of researchers and companies because it is potentially low-cost, can reduce material waste, can require less energy, and is easy to integrate [1], [2], [3], [4], [5]. PE includes all the printing methods consisting of the deposition of functional inks or pastes to print the desired pattern on a wide range of substrates. Therefore, PE can fabricate sensors, flexible batteries, antennas, and electronics [6], [7], [8] by using substrates and functional inks or pastes with nonconventional properties, such as flexibility, stretchability, transparency, and biocompatibility [9], [10]. In this way, it is possible to extend the use of electronic devices to numerous new applications, from biomedical to agricultural and industrial sectors [11], [12]. Several technologies belonging to PE can fabricate electronic devices on 3-D surfaces [2], paving the way to produce smart objects, i.e., objects that integrate sensors and electronics to sense and/or modify the surrounding environment [13]. Piezo-driven jet valve dispensing, also called Piezojet, is a printing method for depositing inks and pastes with a viscosity below 200 000 cP. Piezojet is a drop-on-demand and noncontact method. It is based on the ejection of droplets from the nozzle of 50–300 μm diameter due to the pressure generated by a piezo-driven tappet in contact with the ink inside of a small reservoir. Besides electronics, a smart object or device should integrate sensors to enable the monitoring and control of the processes and the environment [14]. In particular, resistive sensors—such as strain sensors, temperature sensors, or gas sensors—fabricated with PE methods have been extensively studied [15], [16], [17]. Piezojet is also a promising technology for fabricating sensors, even on 3-D surfaces and objects, but it is still poorly understood. In the Piezojet process, many parameters contribute to proper sensor fabrication, and they change according to the type of printhead structure (needle shape, piezo stack structure, and so on) and the ink used [18], [19], [20], [21]. Properly controlling the printing process through tuning of printing parameters and defining guidelines for evaluating the influence of these printing parameters is essential to repeatably obtain printed sensors with good performance. Sohn and Choi [19] and Sohn et al. [22] tried to identify the most critical printing parameters to obtain drop with a repeatable minimum volume (and mass) by using a balance, but they did not study the process behavior during normal operation for sensor fabrication.

In this work, we studied the influence of the printing parameters on printed structures and by evaluating the printed features from both geometrical and electrical points of view. In this way, we could define and propose an approach to identify and tune the most critical printing parameters with the aim of improving the printing quality and repeatability of the printing process. In particular, we studied the performance of the Nordson PICO Jetting system, a Piezojet process, mounted on the Neotech PJ15X machine. Since the setting of the printing parameters strictly depends on the ink used, we tested the proposed method by using two conductive inks used in sensor fabrication, both as a sensing layer or for

Manuscript received 14 April 2023; revised 23 September 2023; accepted 18 October 2023. Date of publication 15 November 2023; date of current version 21 December 2023. This study was carried out within the MICS (Made in Italy – Circular and Sustainable) Extended Partnership and received funding from the European Union Next-GenerationEU (PIANO NAZIONALE DI RIPRESA E RESILIENZA (PNRR) – MISSIONE 4 COMPONENTE 2, INVESTIMENTO 1.3 – D.D. 1551.11-10-2022, PE00000004). This manuscript reflects only the authors' views and opinions, neither the European Union nor the European Commission can be considered responsible for them. The Associate Editor coordinating the review process was Dr. Anoop Chandrika Sreekantan. *(Corresponding author: Michela Borghetti.)*

Michela Borghetti, Emilio Sardini, and Mauro Serpelloni are with the Department of Information Engineering, University of Brescia, 25123 Brescia, Italy (e-mail: michela.borghetti@unibs.it; emilio.sardini@unibs.it; mauo.serpelloni@unibs.it).

Valeria Nicolosi and Dahnan Spurling are with the School of Chemistry, Trinity College Dublin, Dublin 2, D02 W9K7 Ireland (e-mail: nicolov@tcd.ie; spurlind@tcd.ie).

Digital Object Identifier 10.1109/TIM.2023.3331397

interconnects, a silver-based ink, and a $Ti_3C_2T_X$-based ink. Silver ink is largely used to fabricate conductive pads for sensors, conductive interconnects, or entire sensors (i.e., strain sensors [23] and temperature sensors [24]). $Ti_3C_2T_X$ ink is a 2-D material analogous to graphene, belonging to the MXene family [25]. MXenes are promising materials due to their extraordinary mechanical, physical, chemical, and optical properties. MXenes, and in particular $Ti_3C_2T_X$, have been extensively studied and used for the fabrication of energy storage devices [26] but also of sensors, such as strain sensors [27], gas sensors [28], and biosensors [29]. The two inks were also deposited on different substrates (glass, plastic, and ceramic) to measure the line profile and evaluate the process settings under different conditions.

II. Fabrication Method

A. Inks and Substrates

In this work, two inks were selected, one silver and one 2-D material ink. LOCTITE ECI 1011 E&C was used to fabricate highly conductive tracks. It is an ink based on small silver particles (less than 2 μm), suitable for flexographic, gravure, and screen printing. It has a viscosity of 2800 cP and shows good adhesion on PET. The recommended drying and sintering temperature in a box oven is 150 °C for 10 min [30]. This ink was chosen because of its high conductivity, especially suitable for pads and conductive paths of sensors. The declared resistance sheet is lower than 0.005 Ω/sq calculated for a film 25 μm thick.

$Ti_3C_2T_X$ aqueous ink with concentration of 40 mg· mL^{-1} was used to fabricate tracks with conductive properties or sensitive layers. It was prepared according to the method proposed in [31], without any dilution. In this case, no curing process after the printing process is required. The expected viscosity is around 200 cP. $Ti_3C_2T_X$ was selected as a representative of 2-D materials, which exhibit interesting sensing, mechanical, and electrical properties.

The inks were printed on three different substrates: glass, ceramic, and plastic. A piece of glass (80 × 50 × 5 mm) was used to deposit the silver tracks and measure their profile. Aluminum oxide (Al_2O_3) sheets (50 × 50 × 0.5 mm) were selected as highly porous substrates to deposit both silver and $Ti_3C_2T_X$ ink. Al_2O_3 suffers from a high level of roughness but allowed us to evaluate the influence of the printing parameters with different substrates typically used to fabricate sensors. Novele IJ-220 sheets (60 × 60 × 0.140 mm), a transparent coated PET substrate, were used as a plastic substrate for $Ti_3C_2T_X$ for line profile measurements. The mesoporous silica coating promotes the adhesion of many electrically conductive inks. In a previous work [31], the adhesion of $Ti_3C_2T_X$ on Al_2O_3 and IJ-220 was demonstrated when $Ti_3C_2T_X$ was printed by aerosol jet printing.

B. Design of the Printed Patterns and Preparation of the Printing Setup

The three patterns shown in Fig. 1 were adopted for the evaluation of the printed features from geometrical and electrical points of view.

*Pattern #*1 (three six 5-mm straight lines) was used to find the proper printing parameters for each ink, while *pattern #*1*a* (six 5-mm straight lines) was used to evaluate the process variability over six repeated prints. Evaluating printed straight and short lines is a representative case since sensors and electronics fabricated by using Piezojet are obtained from the combination of different lines forming polylines, such as grids (as in the strain sensors [32]), combs (as in the gas sensors [33]), or more complex structures [34]. *Pattern #*2 (42-mm lines) was used to evaluate the printing process quality and to measure the resistance of the high conductive silver lines with good accuracy, while *pattern #*3 (serpentine shape), typically used for temperature and strain sensors, was used to evaluate the printing quality of more complex structures.

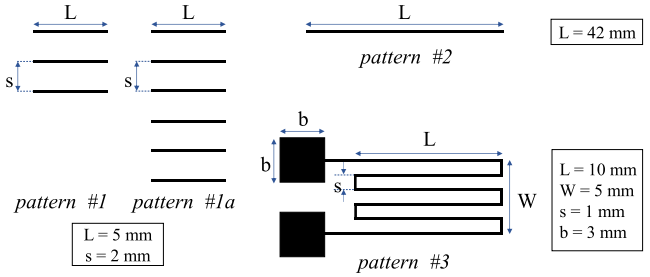

Fig. 1. Patterns and dimensions used for the optimization of the printing process and the evaluation of the printed features.

A software provided by the printer manufacturer was used to draw the designed patterns and convert the Computer-Aided Design and Drafting (CAD) files into motion control files for controlling the printhead movements according to the design pattern.

C. Printing and Curing Process

In this work, we used and tested the PICO Jetting system, a piezo-driven jet valve dispensing system produced by Nordoson, mounted on a PJ15X five-axis functional printer produced by Neotech AMT. The jetting system is composed of: 1) a piezo actuator, which forces the drop formation exiting from the nozzle; 2) a fluid body assembly, which includes the needle connected to the piezo actuator, the valve seat, and the nozzle; and 3) it is connected to the ink supply, a syringe barrel that contains the ink. M5T 3.0S P7 E05 (Nordson) with the nozzle in the seat orifice with a diameter of 50 μm was the fluid body assembly used in this work. A heater is integrated into the proximity of the fluid body assembly to reduce the viscosity of the ink. The tappet (needle) connected to the piezo-driven jet valve is in direct contact with ink inside the reservoir, from which comes out the drop through the nozzle [2]. The mechanism for the drop formation can be divided into four phases: 1) the tappet is in close contact with the nozzle to prevent ink exit since the piezo actuator is powered on with the maximum voltage; 2) the voltage is changed to the minimum value in few milliseconds, the needle starts to rise, and the reservoir starts to fill up with the ink; 3) the needle is at the maximum height and the reservoir is filling up; and 4) the power of the piezo actuator changes again to the maximum value, the needle is lowered toward the reservoir, and a drop of ink is ejected from the nozzle toward the substrate. This mechanism is repeated cyclically

every *Pulse* milliseconds according to the pattern to be printed.

After placing it on the printing plate, the substrate was cleaned with ethanol. The PET substrate was cleaned only with a dry wipe to prevent removal of the coating.

Then, the selected pattern was printed using the associate motion control file generated by the software. The printing process was possibly repeated several times to increase the total thickness of the deposited layers and thus to decrease the resistance of the selected conductive inks.

After printing, the printed samples were thermally cured according to the type of printed ink. In the case of the silver, the samples were cured in an oven at 150 °C for 10 min to promote the sintering of the silver nanoparticles, according to the datasheet. The samples based on $Ti_3C_2T_X$ were cured at 60 °C for 30 min in an oven to promote solvent evaporation.

D. Printing Parameter Setting

The printing process is regulated by the nine parameters listed as follows, whose value mainly depends on the rheological properties of the ink to be deposited.

1) *Close Volts* is the maximum voltage applied to the piezo actuator required to prevent ink exit during phase 1.
2) *Stroke* determines the maximum height of the needle reached at the end of phase 2 and kept in phase 3. It is expressed as a percentage of the *Close Volts* value.
3) *Pulse* is the time required to move the needle from the open to the close position (phase 2).
4) *Open* is the time in which the reservoir is filled (phase 3).
5) *Cycle* is the time to complete the four phases.
6) *Close* is the time required to move the needle from the open to the close position (phase 4).
7) *Pressure* is the pressure inside the syringe and promotes the reservoir filling during phases 2 and 3. The greater the viscosity, the greater should be the pressure value.
8) *Speed* is the printing speed at which the printing plate is moved.
9) *Temperature* is the temperature inside the fluid body assembly regulated by the heater.

In order to guarantee a repeatable and reproducible printing process, a fine control of the volume and shape of the ink drop is required through the tuning of the printing parameters. As confirmed in [35] and [36], the shape and size of the formed droplets depend on the piezoelectric force produced by the piezo actuator through the tappet and the pneumatic force generated by the pressure inside the syringe and thus on the energy transferred to the droplet during the printing process.

The piezoelectric force is mainly determined by *Close Volts* and *Stroke*. The greater their value, the higher the exerted force. Furthermore, in the case of low-viscosity inks, the greater their value, the smaller and more uncontrollable the droplets, generating satellites and undesired spots on the substrate, as confirmed by the experimental results. This phenomenon is typical of inkjet printing when the printing parameters are not set properly for low-viscosity inks [37]. Inkjet drops are formed by squeezing fluid through a tiny hole, the harder the ink is pushed, the higher the stress on the fluid, and thus, drop formation depends on the ink's properties, namely, viscosity, surface tension, and particle content. This phenomenon is also expected in the case of Piezojet. Another parameter influencing the energy transferred to the droplet is *Close* time.

Pulse and *Open* determine the volume of the droplet and the dot size. They depend on the ink properties and on its ability to fill the reservoir under the pressure inside the syringe.

Speed and *Cycle* affect the edge of the printed lines. The greater the *Cycle*, the greater the time between two consecutive ejected drops. The greater the *Speed* value, the wider the spatial distance between two consecutive ejected drops. Their values are optimal if the edges of the line are straight (the line appears as a rectangle). For this reason, *Speed* and *Cycle* can be tuned in the second stage according to the diameter of the deposited droplet (it depends on the volume of the droplet) in order to obtain straight and uniform lines.

Pressure regulates the volume and the pneumatic force on the energy transferred to the droplet and its importance is defined by the ink viscosity, as confirmed in [38]. Lower the viscosity (less than 150 cP), more pneumatic force is relevant. *Temperature* generally regulates the viscosity of the ink promoting the printability of the ink.

III. Printing Parameter Tuning Method

A. Tuning Method

Due to the correlation of printing parameters, the setting of the printing parameters process passes through two stages. The goal of the first stage is to define the most significant parameters and the values of the others. In the first stage, *Temperature*, *Speed*, *Open*, and *Cycle* are kept constant, and their value can be defined starting from values used for other inks with similar viscosity and rheological properties. For example, while $Ti_3C_2T_X$ can be printed at room temperature, silver ink needs a higher temperature to lower its viscosity and increase its printability. Three levels for the other five parameters are defined starting from the literature or previous works and all the possible combinations are tested. As confirmed by the experimental results of Section IV, the three levels should differ by less than 20% to guarantee the formation of the droplet. *Pattern*#1 of Fig. 1 can be used to have replicate lines obtained with the same printing parameter set.

In the second stage, a tuning of the most significant parameters was performed by defining N levels for each parameter. *Pattern #1a* in Fig. 1 can be used to have replicate lines obtained with the same printing parameter set. In that way, a preliminary evaluation of the repeatability can be done.

To define the optimal values of the printing parameters in both stages, the printed lines were evaluated by measuring their features (width and thickness) and by inspecting the region around them for finding undesired isolated spots.

B. Viscosity Measurement Setup, Imaging, Dimensional, and Electrical Measurement

Viscotech VR 3000 MYR modelV2-L, a rotational viscometer, was used to measure the viscosity of noncommercial $Ti_3C_2T_X$ ink and commercial silver ink. The tests were performed at 25 °C, with a speed of 200 r/min and an accuracy of 10 cP.

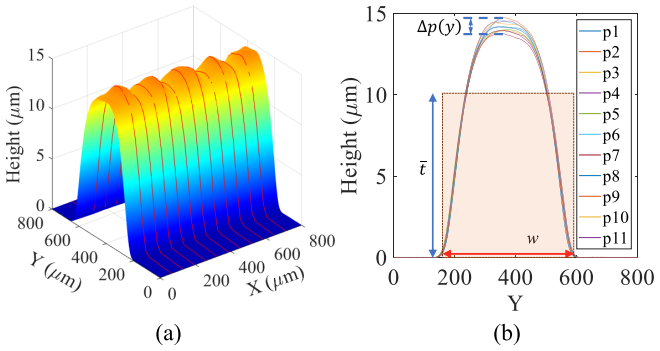

Fig. 2. Surface elaboration of a printed silver line acquired by optical profilometer. (a) 3-D profile and 11 analyzed cross sections (red lines). (b) Overlap of the 11 cross sections and parameters considered for the analysis of the printing quality. The red rectangle has the same area ($w \cdot \bar{t}$) of the average profile $\overline{p(y)}$.

In this work, the effects of the printing parameters on the printed features were evaluated through the analysis of the geometrical aspects (cross section, width, and thickness of the printed lines) and the electrical performance (electrical resistance).

NB50T (Orma Scientific), an optical microscope with a 2× zoomed-in view, equipped with a camera connected to a laptop was used to inspect the printed lines and the area around them. Especially in the case of $Ti_3C_2T_X$ ink, the inspection of the area close to the printed lines was required to detect satellite drops and undesired spots generated when the selected printing parameters were not suitable for a controllable ink ejection.

An optical profilometer and a mechanical profilometer were used to measure the geometrical aspects and thus to preliminary evaluate the repeatability of the printing process and the influence of the printing parameters on the geometry of the printed patterns.

An Alpha-Step IQ Surface Profiler, a diamond stylus-based profilometer operating with an accuracy of 0.1%, was used to measure the profile characteristics of the printed $Ti_3C_2T_X$-based lines and the printed silver lines on Al_2O_3. The stylus was moved along the x-axis, i.e., perpendicular to the printed edge, for 800 μm with steps of 1 μm, while the thickness was obtained by measuring the movement of the stylus along the z-axis, obtaining the curve $z(y)$. The start position and the stop position were defined at least 50 μm before and after the printed line (i.e., in a position without ink). For each line, three profiles $p(y)$ were acquired, one in the middle and the other two one millimeter from the ends of the line.

A Profilm3D (fabricated by Filmetrics), an optical profilometer, was used to evaluate the geometry of the printed silver lines on glass. In this case, 11 profiles $z(y)$ were extracted from each inspected area (800 × 900 μm, resolution of 1.74 μm). The profile corresponds to the cross section of the printed lines (the printed lines are positioned parallel to the x-axis, and hence, the cross section is parallel to the y-axis). For each printed line, three portions of 800 μm were inspected. An example of an acquired portion of the printed silver line is shown in Fig. 2(a).

Once acquired or extracted the profile of the printed line, the baseline b was averaged and leveled considering the measurement points outside the printed line and the profile $p(y)$ of the printed line was corrected in order to have $p(y) = z(y) - b$ and filtered with a standard spline filter, with a cutoff wavelength of 50 μm. From the acquired profile, it was possible to define the following dimensions of the printed line.

1) w, the width, is the span where $p(y)$ is nonzero (considering the roughness of the substrate).
2) $t_{\max}$, the maximum height, is the maximum of $p(y)$.
3) S, the cross-sectional area, is calculated by using a Riemann sum-type approach.
4) $\bar{t}$, the average thickness, is S/w.

Considering lines obtained with the same materials and method, all the analyzed cross sections $p(y)$ were overlapped to find w, $t_{\max}$, S, $\bar{t}$, $\overline{p(y)}$, and their dispersion. An example of the profiles of a printed silver line extracted from the acquired surface [see Fig. 2(a)] is shown in Fig. 2(b).

Finally, a multimeter was used to evaluate the electrical properties of the printed tracks. An HP 34401A, a 61/2 digit multimeter, was used to measure the resistance, R, of the printed lines in a four-terminal configuration. The resistivity ρ of the material was obtained with the equation $\rho = R \cdot S/d$, where S is the mean cross section calculated from the profile measurements and d is the distance between the probes.

IV. Results and Discussion

A. Viscosity Measurements

The viscosity of the silver and $Ti_3C_2T_X$ inks was measured as (2900 ± 10) and (250 ± 10) cP, respectively. The resulting viscosity of LOCTITE ECI 1011 E&C is in accordance with the specification of its datasheet. The measurement of the viscosity of both inks helped to define the starting value for each process parameter.

B. Printing Parameter Tuning for the Silver Ink Deposition

Starting from the manufacturer's suggestions, we defined the starting value and their alternatives for each printing parameter (see Table I) and we tested all the combinations. Some combinations were immediately excluded, i.e., when *Close Volts* = 100 V, *Pressure* = 0.2 bar, and *Stroke* = 60%, reducing the possible combinations to 72. Fig. 3 shows the influence of the *Pressure* on the ink deposition. At 0.5 bar [see Fig. 3(b)], the deposition of the ink is not uniform on the substrate and sometimes no droplets are deposited on the substrate because the chamber is not correctly filled. Similar results were obtained for a lower level of *Stroke*; if *Stroke* is 60%, no droplet is formed, and if *Stroke* is 70%, the deposition is not uniform. The starting values of Table I ensured good control of the drop ejection of the silver ink. In that case, under the microscope, the ink deposition seems to be uniform with the starting value; the printed lines appear straight and the width constant along the line, as designed.

According to the results of the first stage, we decided to perform the second stage and study the influence of the parameters *Cycle* and *Pulse* on the quality of the printed

TABLE I

TESTED VALUES OF THE PRINTING PARAMETERS FOR THE DEPOSITION OF A SILVER INK

Parameter	Starting Value	I Alternative Value	II Alternative Value
***Close Volts* (V)**	107	100	120
***Stroke* (%)**	78	60	70
***Open* (ms)**	0.25	-	-
***Close* (ms)**	0.20	0.3	0.25
***Pulse* (ms)**	0.43	0.50	0.35
***Cycle* (ms)**	12		
***Pressure* (bar)**	1	0.2	0.5
***Speed* (mm/min)**	900	-	-
***Temperature* (°C)**	39	-	-

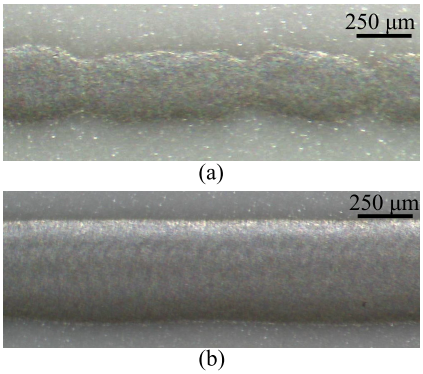

Fig. 3. Influence of *Pressure* on the printed silver line aspect. The printing parameters values are reported in Table I except for *Pressure*. (a) Uniform ink deposition due to the correct setting of printing parameters (*Pressure* is 1 bar). (b) Nonuniform ink deposition due to the wrong setting of printing parameters (*Pressure* is 0.5 bar).

TABLE II

TESTED VALUES OF CYCLE AND PULSE FOR SILVER INK DEPOSITION

Set	*Cycle* (ms)	*Pulse* (ms)
#1	8	0.35
#2	8	0.43
#3	10	0.35
#4	10	0.43
#5	12	0.35
#6	12	0.43
#7	12	0.50

feature from the geometrical point of view, defining three different levels, as indicated in Table II. The values of *Close Volts*, *Stroke*, *Open*, *Close*, *Pressure*, *Speed*, and *Temperature* were kept constant throughout all the tests. Therefore, we defined seven combinations (printing settings), as reported in Table II, and tested the printed features from a geometrical point of view (profile, width, mean, and maximum height). In this test, we deposited silver ink on the glass, and the profile measurements were taken with the optical profilometer. The printed lines were designed according to *pattern* #1. For each setting, we printed six lines. The combinations with *Pulse* equal to 0.5 ms and *Cycle* equal to 8 or 10 ms were not considered because the width of lines increased considerably.

The cross sections of the printed lines acquired by the optical profilometer and evaluated according to the procedure described in Section III-B are shown in Fig. 4. The blue

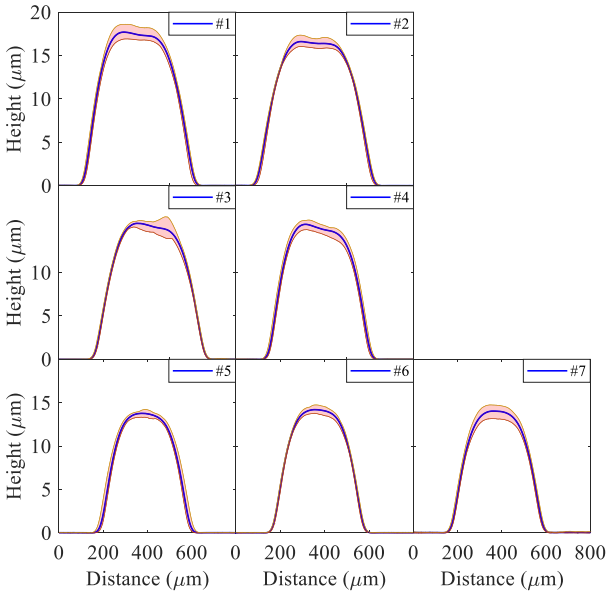

Fig. 4. Mean profile (blue line) and overlap of multiple cross sections of six printed silver lines (red area) grouped according to the used printing setting and listed in Table II (set #1–#7). For each plot, the number of the printing setting is indicated in the legend.

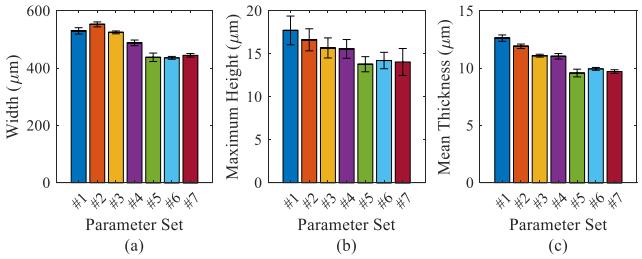

Fig. 5. Mean value and dispersion of (a) w, (b) $t_{\max}$, and (c) $\bar{t}$ calculated on the results shown in Fig. 4 (silver lines on glass group according to the used printing setting listed in Table II).

line (inside the shadow area) represents the mean profile considering all the acquired cross sections of six printed lines, while the shadow area includes all the acquired profiles.

The repeatability of the printed process qualitatively deducted from the width of the shadow area is worse when *Pulse* and *Cycle* are equal to the lowest value (0.35 and 8 ms, respectively), as shown by a wider shadow area ($\Delta p(y) = 2.3\%$). The average w, $t_{\max}$, and $\bar{t}$ and calculated for the 66 cross sections is summarized in Fig. 5. As expected, the lower the *Cycle*, the greater w, $t_{\max}$, and $\bar{t}$; this indicates a larger drop volume. Set #6 (*Cycle* = 12 ms and *Pulse* = 0.43 ms) represents the best compromise in terms of process repeatability; indeed, w and $\bar{t}$ are equal to (435.5 ± 5.0) and (9.9 ± 0.1) μm, respectively. Therefore, the optimization of the process was performed by studying the profile of six lines and minimizing their deviation from the average value.

Similar results (listed in Table III) were obtained when the silver ink was deposited on Al_2O_3, despite its greater roughness.

The calculated average roughness (*Ra*)—defined in ASME B46.1 as the "arithmetic average of the absolute values of

TABLE III
PROFILE MEASUREMENTS OF PRINTED SILVER LINES

	On glass		On Al_2O_3	
***Cycle* (ms)**	***w*** **(μm)**	$\bar{t}$ **(μm)**	***w*** **(μm)**	$\bar{t}$ **(μm)**
0.35	437 ± 15	9.6 ± 0.3	438 ± 20	8.7 ± 0.4
0.43	436 ± 5	9.9 ± 0.1	442 ± 13	8.8 ± 0.3
0.50	444 ± 6	9.7 ± 0.2	432 ± 27	8.9 ± 0.6

the profile height deviations from the mean line, recorded within the evaluation length"—is 0.74 μm for Al_2O_3 and it was obtained by measuring the profile height on a line 1-mm long with the mechanical profilometer. *Ra* of the glass can be considered negligible. The different *Ra* implied an average lower mean thickness and a greater variability in the width and mean thickness, as reported in Table III.

C. Dimensional and Electrical Measurements of Printed Silver Lines After Optimization Process

Once optimized printing parameters, *pattern* #1*a* was used to print straight lines on glass and Al_2O_3. For every six lines, we increased the number of printed overlaid layers (N_{layers}) from one to four to obtain four groups of six lines with $N_{layers} = 1$, 2, 3, and 4, on both substrates. The results are shown in Figs. 6 and 7. As expected, the width and the maximum height increase, and the results are similar for both substrates by increasing N_{layers}. The repeatability of the printing process, qualitatively deduced from the width and dispersion of the shadow area (see Fig. 6) and from the expanded uncertainty U—calculated as the experimental standard deviation on 18 profiles acquired from six identical printed lines and 95% level of confidence (the coverage factor is based on t-distribution) in accordance with the Guide to the expression of uncertainty in measurement (GUM)–-, is better for lines deposited on glass because of the negligible *Ra*. Indeed, in the case of lines deposited on glass, U is 1.5% (4.8% on Al_2O_3) when $N_{layers} = 1$ and decreases to 0.25% (3.3% on Al_2O_3) when $N_{layers} = 4$. Furthermore, in the case of glass, the width and maximum height of the printed lines are greater. For example, $N_{layers} = 4$ w and t are, respectively, 821 and 32 μm in the case of glass and 756 and 28 μm in the case of Al_2O_3. The reason is that, in the case of Al_2O_3, a certain amount of the deposited volume covers the pores of the substrate and this causes a loss of the expected shape of the printed line (the edges are irregular, and thus, the variability of the width along the line increases), as also confirmed in [39]. The mean values of the linewidth, the area, and the maximum height as a function of N_{layers} can be fit with a first-order line with the least squares method for both substrates, weighted with measurement uncertainty. The coefficient of determination R-squared of w is 0.99 in the case of the lines printed on glass and 0.98 in the case of the lines printed on glass Al_2O_3.

In the final test, we estimated the resistivity of the printed lines, by printing *pattern* #2 on glass and with different N_{layers}. Indeed, long lines are required to measure the resistance between the two ends with an accuracy better than 3% since the resistivity of the silver is very low, and the resistance of short lines (5 mm) is expected to be in the low hundreds of milliohms and the accuracy of the multimeter in that range is 16% of the reading in the worst case. As expected, the resistance measured on the length of 40 mm (l) is 559, 280, 192, and 142 mΩ for $N_{layers} = 1$, 2, 3, and 4, respectively. Considering the area of the cross section of the lines measured with the profilometer and by applying the Ohm law ($R = \rho \cdot l/S$), the resistivity ρ is confirmed constant (due to the metallic nature of the ink) and results (0.062 ± 0.002) $\mu\Omega$·m, in accordance with the datasheet specifications.

TABLE IV
TESTED VALUES OF THE PRINTING PARAMETERS FOR THE DEPOSITION OF A $Ti_3C_2T_X$ INK

Parameter	**Starting Value**	**I Alternative Value**	**II Alternative Value**
***Close Volts* (V)**	115	105	120
***Stroke* (%)**	63	58	68
***Open* (ms)**	0.25	-	-
***Close* (ms)**	0.60	0.2	0.40
***Pulse* (ms)**	0.40	0.50	0.30
***Cycle* (ms)**	12		
***Pressure* (bar)**	0.4	0.6	0.8
***Speed* (mm/min)**	900	-	-
***Temperature* (°C)**	24	-	-

D. Printing Parameter Tuning for $Ti_3C_2T_X$ Deposition

Starting from the previous results on inks with similar viscosity, we defined the starting value and their alternatives for each printing parameter (see Table IV).

$Ti_3C_2T_X$ was less viscous than silver ink, and thus, satellites and undesired spots were expected without the optimization of the printing parameters. Indeed, *Stroke* was expected as one of the crucial parameters for the proper deposition of the ink, as shown in Fig. 8. When *Stroke* was 58%, the ink was not able to exit from the nozzle (for this reason, this value was excluded in the systematic tests), while when *Stroke* was 68%, the edges of the printed lines were not regular. The number of undesired isolated spots and the average diameter on the surface were at maximum when the *Stroke* was 68%. This result confirms our assumption that the satellites are produced when the ink has a low viscosity. The value of *Pressure* helps only to increase the width of the lines and does not reduce the number of undesired spots. In order to study the behavior, we tested more levels of pressure, as shown in Fig. 9. The diameter, d, of the desired spots that form the lines linearly increases with pressure p from 220 to 353 μm ($d = 130$ μm/bar·$p + 190$ μm/bar and R-adjusted = 0.997), while the resistance decreases from infinite (at *Pressure* = 0.4 bar) to 455 Ω. A significant difference in the printed line aspect (edge shape) was found when *Close Volts* decreases at 105 V (−8.7%), as shown in Fig. 10. If *Close Volts* is set to 120 V (+4.3%), the ink is not ejected from the nozzle. Low *Close Voltage* (105 V) causes uncontrolled deposition of the ink; in some cases, the amount of the ink is too high (when correlated with *Stroke* = 68%) and the ink is spread over the substrate or the edges are irregular (the width increases along the line). When *Stroke* is set to 63%, by increasing *Pulse* from 0.30 to 0.50 ms (steps of 0.10 ms), the width increases from 230 to 345 μm, but the incidence of

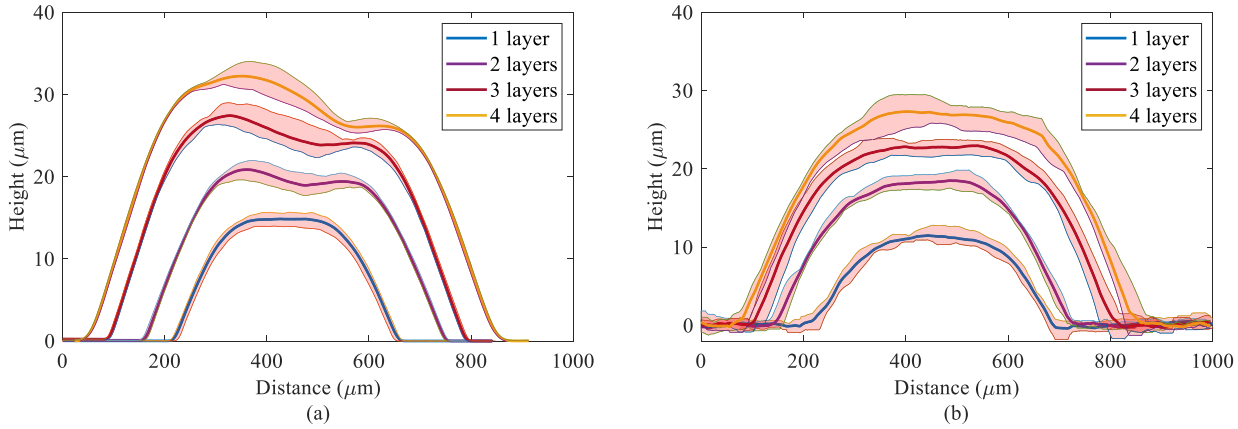

Fig. 6. Mean profile (solid lines) and dispersion (shadow area) of silver lines printed on (a) glass and (b) Al_2O_3, grouped according to the number of printed overlaps (N_{layers} = 1 to 4). Each group includes identical six lines (*pattern #1a* in Fig. 1).

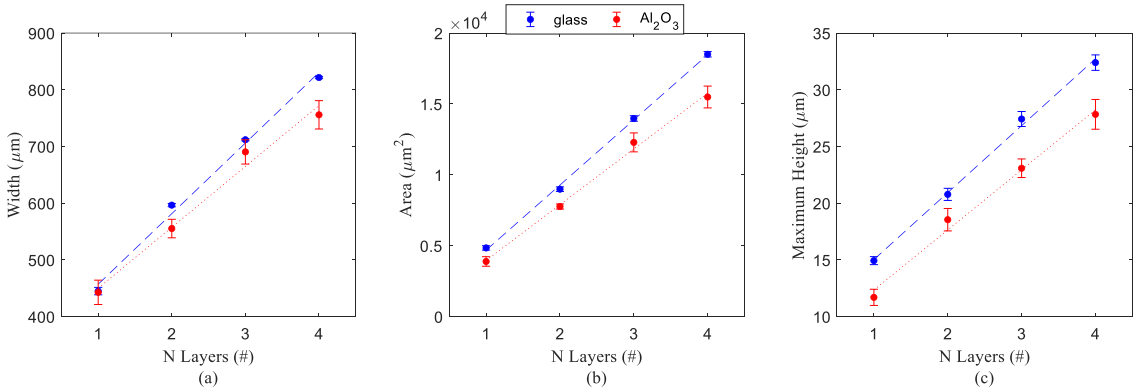

Fig. 7. Mean value (dots) and dispersion (bars) of (a) w, (b) S, and (c) t_{max} calculated on the results shown in Fig. 6, grouped according to the type of substrate and as a function of the number of printed layers N_{layers}. The bars are the expanded uncertainties calculated as experimental standard deviation calculated on 18 measurements and the coverage factor equal to 2.11 (based on t-distribution, level of confidence = 95%), in accordance with the GUM. The dashed lines are the linear regression weighted with measurement uncertainty.

Fig. 8. Effects of *Stroke* (S) on the deposition of $Ti_3C_2T_X$. (*Close Volts* = 115 V, *Pulse* = 0.50 ms, *Close* = 0.4 ms, and *Pressure* = 0.4 bar).

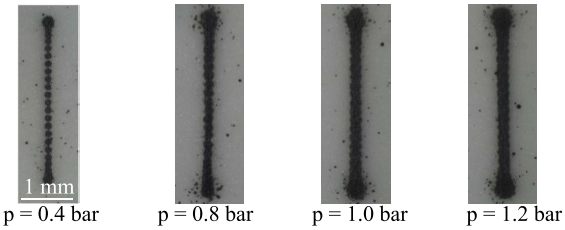

Fig. 9. Effects of *Pressure* (p) on the deposition of $Ti_3C_2T_X$. (*Close Volts* = 115 V, *Stroke* = 63%, *Pulse* = 0.30 ms, and *Close* = 0.4 ms).

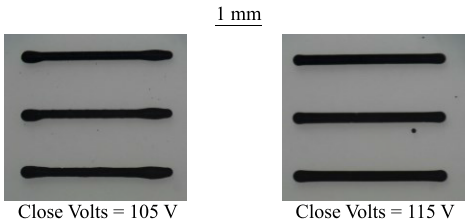

Fig. 10. Effects of *Close Volts* on the deposition of $Ti_3C_2T_X$ on PET (*Stroke* = 63%, *Cycle* = 12 ms, *Close* = 0.6 ms, and *Pressure* = 0.6 bar).

isolated spots is not affected. In order to reduce the incidence of isolated spots at minimum, *Close Volts* should be set to 115 V, *Stroke* should be set to 63%, *Pulse* should be set to 0.40 ms, and *Pressure* should be set to 0.6 bar. In this way, the conduction path for the line is guaranteed. In order to eliminate the isolated spots, *Close* had to be set to 0.6 ms. *Close* is a key parameter to eliminate undesired spots and satellites. In this case, the rheology of ink (including the low viscosity) requires that the needle closes slower.

In order to optimize the printing process, *Speed* and *Cycle* were tuned defining two levels: 600 and 900 mm/min and 12 and 16 ms. The *Speed* and *Cycle* set to 900 mm/min and 16 ms, respectively, significantly affect the edges of the lines because the distance between two consecutive dots is higher than the radius of the dots (see Fig. 11); it is a typical phenomenon when the ratio between *Speed* and the frequency

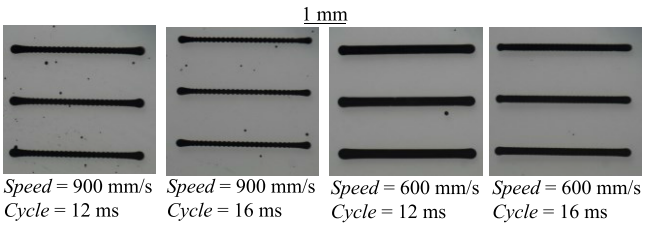

Fig. 11. Effects of *Speed* and *Pulse* on the deposition of $Ti_3C_2T_X$ on PET (*Close Volts* = 115 V, *Stroke* = 63%, *Cycle*= 12 ms, *Close* = 0.6 ms, and *Pressure* = 0.6 bar).

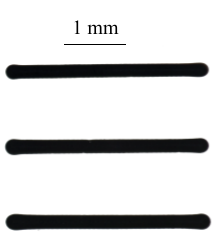

Optimal printing parameter set
Close Volts = 115 V
Stroke = 63 %
Close = 0.6 ms
Cycle = 12 ms
Speed = 600 mm/min
Stroke = 63 %
Open = 0.25 ms
Pulse = 0.4 ms
Pressure = 0.6 bar
Temperature = 25 °C

Fig. 12. Aspect of $Ti_3C_2T_X$ lines printed on PET. On the left are the optimized printing parameters.

of the drop ejection (reciprocal of *Cycle* value) is incorrect. The results described in the text and shown in the pictures are the same when the ink is printed on Al_2O_3 or PET.

The best compromise is obtained when all the printing parameters assume the values shown in Fig. 12. In this case, the overlap of the dots is enough to have straight edges of the line, as well as a narrow enough linewidth. A short width (less than 370 μm) indicates the possibility to obtain fine features and reduced overall dimensions of the printed sensor. According to the manufacturer specifications, the linewidth cannot be lower than 300 μm.

E. Dimensional and Electrical Measurement of Printed $Ti_3C_2T_X$ Lines After Optimization Process

After optimizing the printing parameters, a matrix of 6 × 7 lines (seven columns of *pattern* #1) was printed both on Al_2O_3 and PET. Each column has six identical lines (same N_{layer}) and N_{layer} increases from one to seven across the columns. The geometrical characterization was performed only on the lines deposited on PET because the height of deposited $Ti_3C_2T_X$ is comparable to the roughness of Al_2O_3 and the processing of the acquired data is difficult for the lines with N_{layer} equal or less than six, especially in the width and area measurements. The mean profile and its variability calculated on six identical lines with $N_{\text{layer}} = 7$ are shown in Fig. 13.

The mean values (calculated on six identical lines) related to the cross sections of the $Ti_3C_2T_X$ lines printed on PET as a function of the number of overlap depositions (N_{layer}) are shown in Figs. 14 and 15. As expected, the area and the maximum height of the mean cross section increase linearly with N_{layer} (R-squared = 0.999), whereas the width increases only for $N_{\text{layer}} \leq 4$. The mean width can be considered constant for $N_{\text{layer}} \geq 4$, and it is (477 ± 14) μm. Grouping the

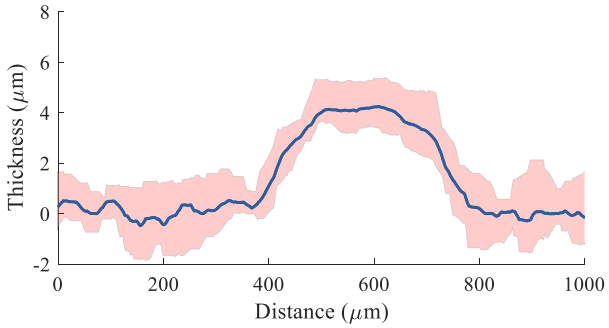

Fig. 13. Mean Profile (solid lines) and dispersion (shadow area) of $Ti_3C_2T_X$ lines ($N_{\text{layer}} = 7$) printed on Al_2O_3. The roughness of the substrate makes difficult the detection of the line profile.

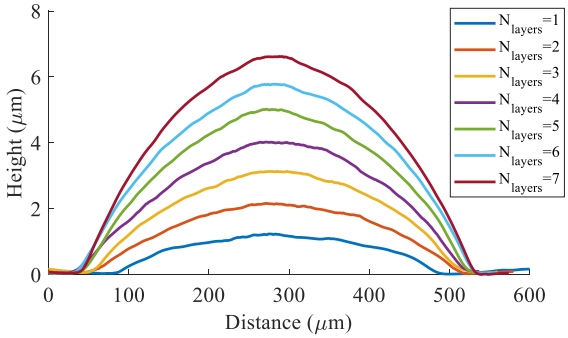

Fig. 14. Mean profile of $Ti_3C_2T_X$ lines (calculated on six identical lines) as a function of N_{layer} (overlap depositions) printed on PET.

measurement according to N_{layer}, the expanded uncertainty U—calculated from the experimental standard deviation on 18 profiles acquired from six identical printed lines and 95% level of confidence—is 4% for $N_{\text{layer}} = 4$ and of less than 1.7% for $N_{\text{layer}} \geq 5$ (±8 μm). These results are also confirmed by area and height measurements. For example, U on the "maximum height" is minimum for $N_{\text{layer}} = 5$ and 6 (±1.2%) and maximum for $N_{\text{layer}} = 3$ (±3.7%). According to these findings, $N_{\text{layer}} = 5$ could be considered the best compromise in terms of repeatability process, ink volume, and line dimensions.

As for silver ink, the substrate affects only the width, thickness, and area of the cross section of the printed lines. For example, when $N_{\text{layer}} = 7$, the width is 415 μm in the case of Al_2O_3—smaller than 479 μm in the case of PET—while the expanded uncertainty U—calculated from the experimental standard deviation on 18 profiles acquired from six identical printed lines and 95% level of confidence (the coverage factor is based on t-distribution)—is 5% in the case of Al_2O_3—greater than 1.5% in the case of PET.

The resistance of all the lines printed on PET and Al_2O_3 was measured (six identical lines for each $N_{\text{layer}} = 1, \ldots, 7$). The ratio of the measured resistance to the length (i.e., the distance of the two probes) as a function of N_{layer} and according to the substrate is summarized in Fig. 16. As for silver lines, the resistance decreases as a function of N_{layer}. The maximum deviation from the mean value calculated on the six identical 3-mm lines is less than 16% when $N_{\text{layer}} = 1$. In the other cases, the deviation is less than ±3.5% for $N_{\text{layer}} = 2$,

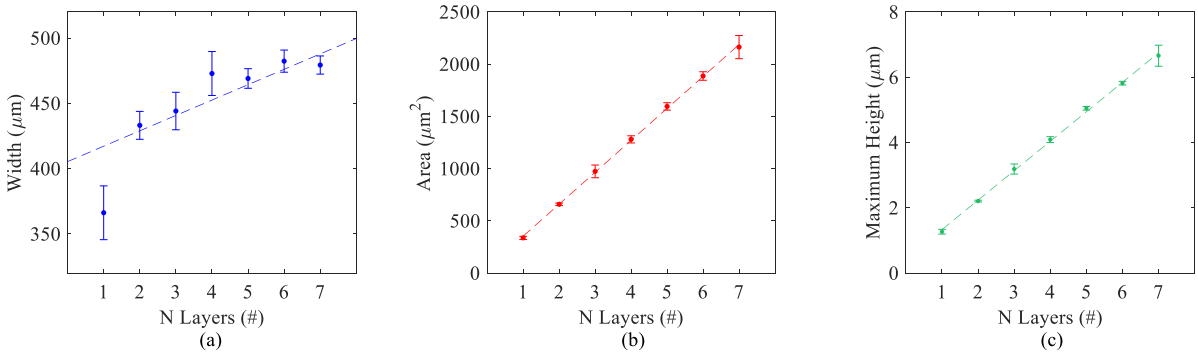

Fig. 15. Mean values (dots) and uncertainties (bars) of (a) w, (b) S, and (c) t_{max} calculated on the results shown in Fig. 14, grouped according to the type of substrate and as a function of the number of printed layers N_{layers}. The bars are the experimental uncertainties calculated as experimental standard deviation calculated on 18 measurements and the coverage factor equal to 2.11 (based on t-distribution, 95% level of confidence), in accordance with the GUM. The dashed lines are the linear regression weighted with measurement uncertainty.

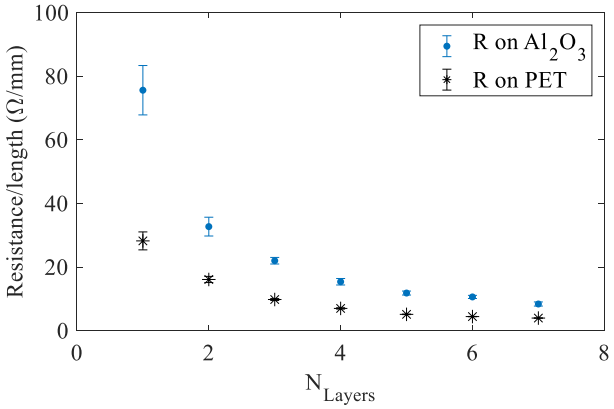

Fig. 16. Mean values (dots) and dispersion (bars) of the ratio of the measured resistance to the length of $Ti_3C_2T_X$ lines on Al_2O_3 and PET.

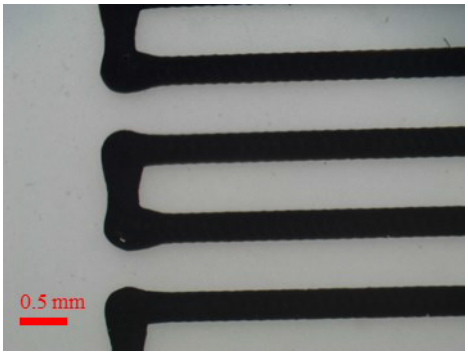

Fig. 17. Details of *Pattern* #3 printed with $Ti_3C_2T_X$ ink on PET.

3 and ±1.5% for $N_{layer} > 3$ both on PET and Al_2O_3. The resistivity is (9.0 ± 0.4) μΩ·m in all the cases, considering the resistance R and the profile measurements S and using the Ohm law $R = \rho \cdot l/S$. The same results in terms of resistance and profile were obtained when *Pattern* #2 was printed on PET. According to these results, despite the long length of the line (42 mm), the deposition can be considered uniform along it.

In the final test, the ability to print more complex geometries was tested. *Pattern* #3 was printed with $Ti_3C_2T_X$ ink on PET. A detail of the printed serpentine is shown in Fig. 17. The technology is also able to print long lines and patterns that required direction changes of the printhead of 90°, contrary to other technologies that require smoother direction changes, such as aerosol jet printing [14]. To obtain these results, abrupt decelerations/accelerations in correspondence with the corners are required and this causes an increase in the ink amount deposited close to the corner: near the corners, the line is visible wider. The measured resistance is (2612.00 ± 60.00) Ω, calculated on six printed serpentine and considering the maximum deviation from the average value. Starting from the Ohm law ($R = \rho \cdot l/S$), measuring the area of the cross section, knowing the average path length l and the resistivity of $Ti_3C_2T_X$ found in the previous test, the calculated resistance is in accordance with the results obtained in the previous tests where straight lines were evaluated. Furthermore, the resistance deviation from the average value calculated on six serpentines is less than 1.5% and this value can be used to estimate the process repeatability.

V. Conclusion

In this work, the performance of the piezo-driven jet valve dispensing (called also Piezojet) was studied for the fabrication of resistive sensors by depositing silver ink and $Ti_3C_2T_X$ ink on different substrates to provide a method for detecting and tuning the most critical printing parameters. The proposed method is divided into two stages. The evaluation of the best printing parameter set is performed through optical inspection and dimensional measurements of printed lines. The first stage of the optimization defines the setting of most of the parameters to obtain the ink ejection and to have a uniform deposition (regarding the deposited volume and the regular edges), while in the second stage, only two parameters were tuned to optimize the process. The results demonstrated that the critical printing parameters depend on the ink, but not on the substrate, as expected. The substrate influences the final aspect of the printed lines due to its roughness and surface tension. For example, silver lines on glass and $Ti_3C_2T_X$ lines on PET have a greater width and maximum height than lines on Al_2O_3 but a lower variability (<±1.5%), considering the uncertainty calculated from the experimental standard deviation.

In the case of silver ink, while *Close Volts* and *Stroke* should set to a particular value for the correct formation of the droplet, *Pressure* is critical to obtain a line with regular edges. The optimization was performed in the second stage by

changing *Cycle* by ±33% (starting value 12 ms) and the *Pulse* by ±8% (starting value = 0.43 ms) to reduce the variability in the area of the printed line cross section. The linewidth and the average thickness were found to be almost constant regardless of the value of the parameters, while the deviation increased when the value of the parameters was different from the starting value. We also found that the average thickness of the lines can be increased from 8.7 to 20 μm by depositing several overlapped ink layers from one to four, with a resulting increase in the width and variability. In the case of silver ink, one deposition is enough to obtain good conductance of the printed line. The resistivity calculated on a 42-mm line is 0.062 $\mu\Omega$·m.

In the case of $Ti_3C_2T_X$ ink, we found that the low viscosity of the ink affects the printing quality when the printing parameters are not optimized; Piezojet, as in inkjet, produces satellites and undesired spots when the viscosity is low, as seen in $Ti_3C_2T_X$ ink (equal to 250 cP), while in the case of silver ink, this did not occur. *Close* was found to be a critical parameter for $Ti_3C_2T_X$: shorter *Close* causes undesired spots, while *Stroke* and *Close Volts* must assume a specific value to deposit lines with straight edges. *Pressure* and *Temperature* are not as critical as for silver ink because the viscosity is lower. Also, in this case, it is possible to deposit more overlapped layers to reduce the resistance of the printed line, considering that the resistivity of $Ti_3C_2T_X$ (equal to 9.1 $\mu\Omega$· m) and the thickness of the printed line (equal to 1.5 μm with two layers). In particular, at least five layers are recommended to reduce the variability among the printed lines in terms of geometrical dimensions and electrical resistance.

The repeatability of the printing process, expressed here as the standard deviation calculated on the profile of six printed lines, is similar for both inks on glass (±5 μm) or PET (±12 μm).

In the ongoing work, we are fabricating and testing strain sensors based on $Ti_3C_2T_X$, to define the performance of the sensors in terms of sensitivity to the induced strain and the drift due to the temperature. The reproducibility of the printing process with the optimized parameter has been preliminary tested by using the same printing system but in different laboratories and at separate times. Preliminary tests have already been performed with good results confirming the reproducibility. Further analysis can still be done, and the scientific community is sensitized to deepening the reproducibility of the printing process and the proposed tuning method.

ACKNOWLEDGMENT

This manuscript reflects only the authors' views and opinions, and neither the European Union nor the European Commission can be considered responsible for them.

REFERENCES

[1] S. Khan, L. Lorenzelli, and R. S. Dahiya, "Technologies for printing sensors and electronics over large flexible substrates: A review," *IEEE Sensors J.*, vol. 15, no. 6, pp. 3164–3185, Jun. 2015, doi: 10.1109/JSEN.2014.2375203.

[2] P. Bellitti, M. Borghetti, E. Cantù, E. Sardini, and M. Serpelloni, "Resistive sensors for smart objects: Analysis on printing techniques," *IEEE Trans. Instrum. Meas.*, vol. 71, pp. 1–15, 2022, doi: 10.1109/TIM.2022.3181941.

[3] B. Andò, S. Baglio, C. O. Lombardo, V. Marletta, and A. Pistorio, "A low-cost accelerometer developed by inkjet printing technology," *IEEE Trans. Instrum. Meas.*, vol. 65, no. 5, pp. 1242–1248, May 2016, doi: 10.1109/TIM.2015.2490998.

[4] S. A. Alves et al., "Improved tribocorrosion performance of bio-functionalized TiO_2 nanotubes under two-cycle sliding actions in artificial saliva," *J. Mech. Behav. Biomed. Mater.*, vol. 80, pp. 143–154, Apr. 2018, doi: 10.1016/j.jmbbm.2018.01.038.

[5] M. Borghetti and E. Cantù, "Preliminary study on a strain sensor printed on 3D-plastic surfaces for smart devices," in *Proc. Int. Workshop Metrology Ind. 4.0 IoT (MetroInd4.0&IoT)*, Jun. 2019, pp. 249–253, doi: 10.1109/METROI4.2019.8792896.

[6] K. P. Srinivasan, T. Muthuramalingam, and A. H. Elsheikh, "A review of flexible printed sensors for automotive infotainment systems," *Arch. Civil Mech. Eng.*, vol. 23, no. 1, p. 67, Jan. 2023, doi: 10.1007/s43452-023-00604-y.

[7] B. Clement et al., "Recent advances in printed thin-film batteries," *Engineering*, vol. 13, pp. 238–261, Jun. 2022, doi: 10.1016/j.eng.2022.04.002.

[8] J. Chang, X. Zhang, T. Ge, and J. Zhou, "Fully printed electronics on flexible substrates: High gain amplifiers and DAC," *Organic Electron.*, vol. 15, no. 3, pp. 701–710, Mar. 2014, doi: 10.1016/j.orgel.2013.12.027.

[9] J. Zikulnig, S. Lengger, L. Rauter, L. Neumaier, S. Carrara, and J. Kosel, "Sustainable printed chitosan-based humidity sensor on flexible biocompatible polymer substrate," *IEEE Sensors Lett.*, vol. 6, no. 12, pp. 1–4, Dec. 2022, doi: 10.1109/LSENS.2022.3224768.

[10] M. Borghetti, M. Ghittorelli, E. Sardini, M. Serpelloni, and F. Torricelli, "Electrical characterization of PEDOT:PSS strips deposited by inkjet printing on plastic foil for sensor manufacturing," *IEEE Trans. Instrum. Meas.*, vol. 65, no. 9, pp. 2137–2144, Sep. 2016, doi: 10.1109/TIM.2016.2571518.

[11] M. Salve, A. Mandal, K. Amreen, B. V. V. S. N. P. Rao, P. K. Pattnaik, and S. Goel, "A portable 3-D printed electrochemiluminescence platform with pencil graphite electrodes for point-of-care multiplexed analysis with smartphone-based read out," *IEEE Trans. Instrum. Meas.*, vol. 70, pp. 1–10, 2021, doi: 10.1109/TIM.2020.3023211.

[12] R. Rayhana, G. G. Xiao, and Z. Liu, "Printed sensor technologies for monitoring applications in smart farming: A review," *IEEE Trans. Instrum. Meas.*, vol. 70, pp. 1–19, 2021, doi: 10.1109/TIM.2021.3112234.

[13] M. Borghetti, E. Cantù, E. Sardini, and M. Serpelloni, "Printed sensors for smart objects in Industry 4.0," in *Proc. IEEE 6th Int. Forum Res. Technol. Soc. Ind. (RTSI)*, Sep. 2021, pp. 57–62, doi: 10.1109/RTSI50628.2021.9597209.

[14] M. Borghetti, E. Cantù, E. Sardini, and M. Serpelloni, "Future sensors for smart objects by printing technologies in Industry 4.0 scenario," *Energies*, vol. 13, no. 22, p. 5916, Nov. 2020, doi: 10.3390/en13225916.

[15] M. Borghetti, E. Sardini, and M. Serpelloni, "Preliminary study of resistive sensors in inkjet technology for force measurements in biomedical applications," in *Proc. IEEE 11th Int. Multi-Conf. Syst., Signals Devices (SSD)*, Feb. 2014, pp. 1–4, doi: 10.1109/SSD.2014.6808790.

[16] X. Zhang et al., "Printed carbon nanotubes-based flexible resistive humidity sensor," *IEEE Sensors J.*, vol. 20, no. 21, pp. 12592–12601, Nov. 2020, doi: 10.1109/JSEN.2020.3002951.

[17] F. Fatani, M. Vaseem, Z. Akhter, R. M. Bilal, and A. Shamim, "Remote monitoring of skin temperature through a wristband employing a printed VO sensor," *IEEE Sensors J.*, vol. 23, no. 1, pp. 169–180, Jan. 2023, doi: 10.1109/JSEN.2022.3223947.

[18] S. Lu, X. Chen, H. Zheng, Y. Zhao, and Y. Long, "Simulation and experiment on droplet volume for the needle-type piezoelectric jetting dispenser," *Micromachines*, vol. 10, no. 9, p. 623, Sep. 2019, doi: 10.3390/mi10090623.

[19] J. W. Sohn, J. Jeon, M. Choi, and S.-B. Choi, "Critical operating factors of a jetting dispenser driven by piezostack actuators: Statistical analysis of experimental results," *J. Adhes. Sci. Technol.*, vol. 32, no. 4, pp. 359–374, Feb. 2018, doi: 10.1080/01694243.2017.1356210.

[20] J. Ledesma-Fernandez, C. Tuck, and R. Hague, "High viscosity jetting of conductive and dielectric pastes for printed electronics," in *Proc. 26th Annu. Int. Solid Free. Fabr. Symp. Addit. Manuf. Conf. (SFF)*, vol. 2015, pp. 40–55, 2020.

[21] T. Genco, M. Linke, and R. Lammering, "Piezo-driven jet valve dispensing of carbon nanotube-loaded composites: Optimisation and characterisation," *Nanocomposites*, vol. 7, no. 1, pp. 200–214, Jan. 2021, doi: 10.1080/20550324.2021.2004702.

[22] J. Sohn and S.-B. Choi, "Identification of operating parameters most strongly influencing the jetting performance in a piezoelectric actuator-driven dispenser," *Appl. Sci.*, vol. 8, no. 2, p. 243, Feb. 2018, doi: 10.3390/app8020243.
[23] D. Ratnayake, A. Curry, and K. Walsh, "Demonstrating a new ink material for aerosol printing conductive traces and custom strain gauges on flexible surfaces," in *Proc. IEEE Int. Conf. Flexible Printable Sensors Syst. (FLEPS)*, Jun. 2021, pp. 1–4, doi: 10.1109/FLEPS51544.2021.9469773.
[24] M. Georgas, P. Selinis, G. Zardalidis, and F. Farmakis, "Temperature sensors by inkjet printing compatible with flexible substrates: A review," *IEEE Sensors J.*, vol. 23, no. 1, pp. 21–33, Jan. 2023, doi: 10.1109/JSEN.2022.3213072.
[25] J.-C. Lei, X. Zhang, and Z. Zhou, "Recent advances in MXene: Preparation, properties, and applications," *Frontiers Phys.*, vol. 10, no. 3, pp. 276–286, Jun. 2015, doi: 10.1007/s11467-015-0493-x.
[26] M. Mariano et al., "Solution-processed titanium carbide MXene films examined as highly transparent conductors," *Nanoscale*, vol. 8, no. 36, pp. 16371–16378, 2016, doi: 10.1039/c6nr03682a.
[27] L. Yuan et al., "Flexible and breathable strain sensor with high performance based on MXene/nylon fabric network," *Sens. Actuators A, Phys.*, vol. 315, Nov. 2020, Art. no. 112192, doi: 10.1016/j.sna.2020.112192.
[28] N. J. Prakash and B. Kandasubramanian, "Nanocomposites of MXene for industrial applications," *J. Alloys Compounds*, vol. 862, May 2021, Art. no. 158547, doi: 10.1016/j.jallcom.2020.158547.
[29] A. Sinha et al., "MXene: An emerging material for sensing and biosensing," *TrAC Trends Anal. Chem.*, vol. 105, pp. 424–435, Aug. 2018, doi: 10.1016/j.trac.2018.05.021.
[30] *Loctite ECI 1011 E&C*, Loctite, Düsseldorf, Germany, 2022.
[31] M. Borghetti, M. Serpelloni, E. Sardini, D. Spurling, and V. Nicolosi, "Temperature influence on $Ti_3C_2T_x$ lines printed by aerosol jet printing," *Sens. Actuators A, Phys.*, vol. 332, Dec. 2021, Art. no. 113185, doi: 10.1016/j.sna.2021.113185.
[32] Y. Ye, S. Wan, S. Li, and X. He, "Mechanical wind sensor based on additive manufacturing technology," *IEEE Trans. Instrum. Meas.*, vol. 71, pp. 1–8, 2022, doi: 10.1109/TIM.2022.3189732.
[33] M. Borghetti, E. Cantù, A. Ponzoni, E. Sardini, and M. Serpelloni, "Aerosol jet printed and photonic cured paper-based ammonia sensor for food smart packaging," *IEEE Trans. Instrum. Meas.*, vol. 71, pp. 1–10, 2022, doi: 10.1109/TIM.2022.3161695.
[34] C.-Y. Chen, C.-L. Chen, and S.-K. Hung, "Design and implementation of a PCB-based torque sensor with a spiral sensing pattern," *IEEE Trans. Instrum. Meas.*, vol. 72, pp. 1–7, 2023, doi: 10.1109/TIM.2023.3241992.
[35] F. Liravi and E. Toyserkani, "A hybrid additive manufacturing method for the fabrication of silicone bio-structures: 3D printing optimization and surface characterization," *Mater. Design*, vol. 138, pp. 46–61, Jan. 2018, doi: 10.1016/j.matdes.2017.10.051.
[36] M. Piovarči, M. Foshey, V. Babaei, S. Rusinkiewicz, W. Matusik, and P. Didyk, "Towards spatially varying gloss reproduction for 3D printing," *ACM Trans. Graph.*, vol. 39, no. 6, pp. 1–13, Dec. 2020, doi: 10.1145/3414685.3417850.
[37] Y. Zhang, G. Hu, Y. Liu, J. Wang, G. Yang, and D. Li, "Suppression and utilization of satellite droplets for inkjet printing: A review," *Processes*, vol. 10, no. 5, p. 932, May 2022, doi: 10.3390/pr10050932.
[38] H. Yang et al., "High viscosity jetting system for 3D reactive inkjet printing," in *Proc. Int. Solid Freeform Fabr. Symp.*, 2013, pp. 505–513.
[39] D. Valdec, K. Hajdek, I. Majnarić, and D. Čerepinko, "Influence of printing substrate on quality of line and text reproduction in flexography," *Appl. Sci.*, vol. 11, no. 17, p. 7827, Aug. 2021, doi: 10.3390/app11177827.

Michela Borghetti (Member, IEEE) received the master's degree (cum laude) in electronic engineering and the Ph.D. degree in technology for health from the University of Brescia, Brescia, Italy, in 2012 and 2016, respectively.

In 2015, she was a Visiting Ph.D. Student at Universitat Politècnica de Catalunya, Barcelona, Spain. She is currently a Post-Doctoral Researcher with the Department of Information Engineering, University of Brescia. Her research interests include designs and fabrication of sensors for healthcare using innovative printing technologies.

Valeria Nicolosi received the B.Sc. degree in chemistry from the University of Catania, Catania, Italy, in 2001, and the Ph.D. degree in physics from Trinity College Dublin, Dublin, Ireland, in 2006.

In 2007, she moved to the University of Oxford, Oxford, U.K., where she held a Royal Academy of Engineering/EPSRC Fellowship. In 2012, she returned to Trinity College Dublin as an ERC Research Professor at TCD. In 2017, she was promoted to the Chair of Nanomaterials and Advanced Microscopy. She is currently a PI at the Science Foundation Ireland Advanced Materials and BioEngineering Research (AMBER) Centre.

Emilio Sardini (Member, IEEE) received the M.Sc. degree in electronic engineering from the Polytechnic of Milan, Milan, Italy, in 1983.

Since 1984, he has been conducting research and teaching activities at the Department of Electronics for Automation, University of Brescia, Brescia, Italy. Since 2006, he has been a Full Professor of electrical and electronic measurement. He is an author or coauthor of more than 100 articles published in international journals. He has done intensive research in the field of electronic instrumentation, sensors, and signal-conditioning electronics. Recently, research has addressed the development of autonomous sensors for biomedical applications with some specific interests, including devices implantable inside the human body.

Mauro Serpelloni (Member, IEEE) received the M.Sc. degree in management engineering and the Ph.D. degree in electronic instrumentation from the University of Brescia, Brescia, Italy, in 2003 and 2006, respectively.

Since 2010, he has been an Associate Professor with the Department of Information Engineering, University of Brescia. He is the Manager of the New Laboratory for Aerosol Jet Printing. His research interests include electronic instrumentation, sensors, contactless transmissions between sensors and electronics, and signal processing for microelectromechanical systems. Recently, research has addressed the development of wearable sensors, autonomous sensors for biomedical applications, and devices implantable inside the human body.

Dahnan Spurling received the Ph.D. degree in chemistry from Trinity College Dublin, Dublin, Ireland, in 2023.

He is currently working as a Post-Doctoral Researcher for the EIC Transition Project, SuperHEART. His research interests include synthesis of 2-D MXenes and their applications in energy storage.

Open Access funding provided by 'Università degli Studi di Brescia' within the CRUI CARE Agreement